The American Journal of Pathology, Vol. 175, No. 2, August 2009

DOI: 10.2353/ajpath.2009.081034

Neurobiology

Infiltrating CTLs in Human Glioblastoma Establish Immunological Synapses with Tumorigenic Cells

Carlos Barcia, Jr,*† Aurora Gómez,*† José M. Gallego-Sanchez,‡ Ana Perez-Vallés,§ Maria G. Castro,¶ Pedro R. Lowenstein,¶ Carlos Barcia, Sr,‡ and Maria-Trinidad Herrero*†

From the Clinical and Experimental Neuroscience, Centro de Investigación Biomédica en Red sobre Enfermedades Neurodegenerativas,† School of Medicine, University of Murcia, Campus de Espinardo, Murcia, Spain; the Departments of Neurosurgery,‡ and Pathology,§ Hospital General Universitario de Valencia, Valencia, Spain; and the Board of Governors' Gene Therapeutics Research Institute,¶ Cedars-Sinai Medical Center, Los Angeles, and the Departments of Medicine and Molecular and Medical Pharmacology, David Geffen School of Medicine, University of California Los Angeles, Los Angeles, California*

The immunological synapse between T cells and tumor cells is believed to be important for effective tumor clearance. However, the immunological synapse has never been imaged or analyzed in detail in human tissue. In this work, intercellular interactions between T cells and tumor cells were analyzed in detail in human glioblastoma. After characterization of the population of infiltrating T cells by multiple immunofluorescence staining and stereological quantification, the microanatomy of T cell-tumor cell intercellular communication was analyzed in detail using confocal microscopy and three-dimensional rendering. Cytotoxic T lymphocytes that infiltrated human glioblastoma underwent rearrangement when in contact with tumor cells, to form a three-dimensional structure in the intercellular contact area; this was characterized by microclusters of the CD3/TCR complex, re-arrangement of the cytoskeleton, and granzyme B polarization. In addition, such T cell-targeted cells show fragmentation of the microtubular system and increased expression levels of cleaved caspase 3, which suggests that cytotoxic T lymphocytes likely provoke changes in tumor cells and subsequently induce cell death. These results show that the formation of the cytotoxic T lymphocyte immunological synapse occurs in human tissue and may be relevant for the effective immune-mediated clearance of tumorigenic cells, therefore opening up new avenues for glioblastoma immunotherapy. ***(Am J Pathol 2009, 175:786–798; DOI: 10.2353/ajpath.2009.081034)***

Cytotoxic T lymphocytes (CTL) facilitate the specific killing of target cells by forming a complex structure, the immunological synapse (IS).[1–3] After T cell receptor (TCR) signaling, T cells undergo massive conformational changes characterized by the three-dimensional arrangements of membrane molecules and polarization of cellular organelles toward the area of intercellular contact.[4–7] After antigen recognition, CD3/TCR complex is recruited to the area of contact where it forms a central cluster. This is followed by rearrangement of the T cell cytoskeleton, which is crucial for granule-mediated secretion.[5,7–11] The TCR rich central area is surrounded by a ring of lymphocyte function associated (LFA)-1 molecules clustered in the peripheral area of intercellular contact.[6] Importantly, this peripheral cluster formation also involves the cytoskeleton since LFA-1 molecules are connected to the F-actin filaments through Talin molecules, forming a peripheral ring around the central TCR cluster equivalent to LFA-1.[12]

Tumor cells are one of the targets of the immune system.[1] In fact, many tumors, including glioma, are usually infiltrated by T cells.[13–15] Previous studies, performed in tumor animal models *in vivo*, revealed that CTL make contact with tumor cells, where they induce apoptosis.[16,17] However, tumor-infiltrated T cells have scarcely been studied in human tissue *in situ* and their exact function is not well understood. In the present work, we image the intercellular communication between T cells

Supported by grants from the Spanish Ministry of Science (SAF 2004 07656 C02-02), Fundación Séneca (FS/05662/PI/07) and CIBERNED (Centro de Investigación Biomédica en Red sobre Enfermedades Neurodegenerativas).

Note: Figures were reproduced from original RGB images and may appear more accurately online at *http://ajp.amjpathol.org*.

Accepted for publication April 23, 2009.

Supplemental material for this article can be found on *http:// ajp.amjpathol.org.*

Address reprint requests to Carlos Barcia, Clinical and Experimental Neuroscience, CIBERNED, School of Medicine, University of Murcia, Campus de Espinardo, 30071, Murcia, Spain. E-mail: barcia@um.es.

and tumor cells in specimens obtained from patients with glioblastoma multiforme (GBM). We characterize *in situ* the T cell infiltration occurring in tumor areas and image the CD3/TCR polarization-clustering and the microtubular arrangement of the cells, analyzing the α-tubulin cytoskeleton, the microtubule organizing center (MTOC) and the F-actin filaments. This study is the first evidence of IS formation in human tissue and suggests that microcluster rearrangement and cell polarity in T cells may be crucial for an effective immune response *in vivo*, opening up new therapeutic perspectives for GBM treatment through the stimulation of IS formation.

Materials and Methods

Patients and Samples

Four patients from the General Hospital of Valencia (Spain) were diagnosed with GBM and were cited for intracranial surgery. The four cases showed the typical features of GBM, with the classic clinical evolution, neuroimaging, spectroscopy, and anatomo-pathological study (Figure 1). One of the cases (case HC484) was undergoing surgery for the second time. Case HC481 was diagnosed as an astrocytoma grade II with stereotaxic biopsy, which became malignant three years later. Surgery was performed and a second biopsy was obtained for this study. The study was performed according to the approved protocols of all of the institutions involved.

Blood analysis revealed moderate leucocytosis in three cases (near 10,500) with a higher number of neutrophils than lymphocytes: ratio 9:1 (normal ratio: 7.5:2.5). The carcinoembryonic antigen was only expressed slightly in one case. The acute phase proteins were slightly increased in two cases (C-reactive protein and speed of sedimentation). The brain tumors presented a characteristic GBM morphology. Sections stained with H&E showed marked cellularity with hyperchromatism and pleomorphism, with aberrant mitosis. Sections also showed gemistocytic differentiation, gomeruloid vessels, and necrotic palisades (Figure 1).

Tumors were excised with minimal manipulation (before alteration by electrical coagulation) and 2.5 ml of tumor specimens were taken and immersed immediately in 4% paraformaldehyde and 1 week later were washed in 0.1 M/L PBS, pH 7.4, and stored in PBS with 0.1% sodium azide until sectioning. Samples were sectioned by vibratome (Leica Microsystems, Wetzlar, Germany) into 60-μm sections. The biopsy included the different layers of the tumor (from normal tissue to necrotic areas).

Immunocytochemical Procedures

The 60-μm tumor sections were cut serially through the entire sample, and immunofluorescence or diaminobenzidine detection was performed as described previously,[4,18,19] using the following primary antibodies: human

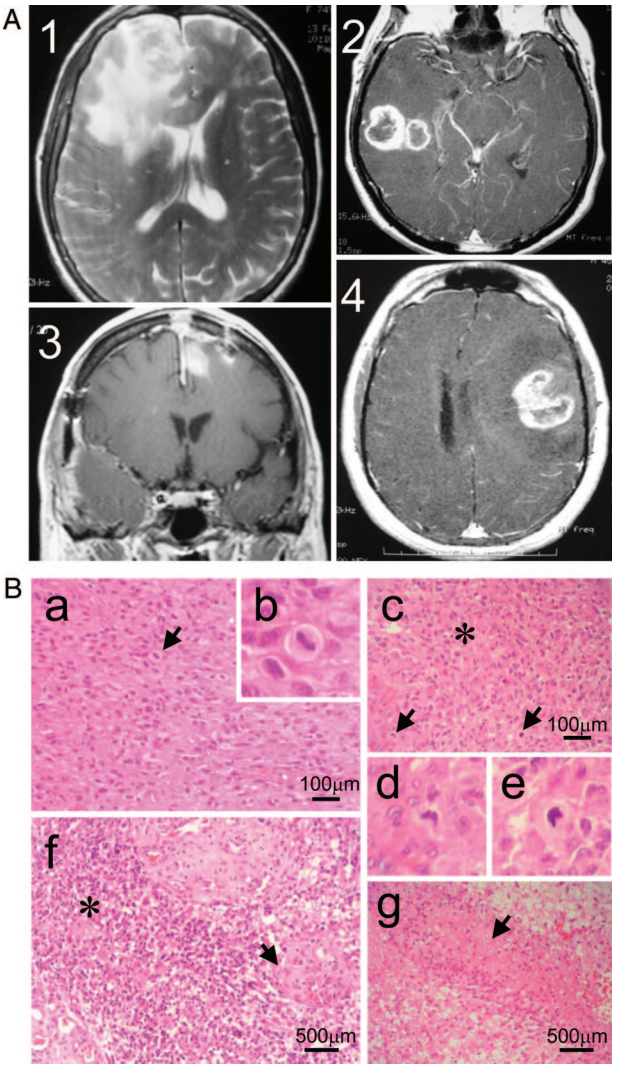

Figure 1. The four cases analyzed show typical features of GBM. **A:** MRI of the four cases of GBM before surgery. A single tumor was located in the frontal lobe in HC484 (**1**) and HC481 (**3**), and in the temporal lobe in HC702 (**2**), while case HC544 (**4**) presented two tumors, one in the **right** temporal lobe and a small one in the **left** frontal parasagittal area. The compression of the ventricles was evident in cases 1, 3, and 4. **B:** Brain Tumors presented a characteristic GBM morphology. Sections stained with H&E showed marked cellularity with hyperchromatism and pleomorphism (picture **a** from case **1**), with aberrant mitosis (indicated by **arrows** in pictures **a** and **c** from cases 1 and **2**, respectively). Higher magnification of the mitosis is depicted in **b**, **d**, and **e**). Sections also showed gemistocytic differentiation (**asterisk** in picture **c** and **f** from cases **2** and **3**, respectively), gomeruloid vessels (**arrow** in **f**) and necrotic palisades (**arrow** in picture **g** from case **4**).

CD3 (1:100, Rabbit, Dako, Glostrup, Denmark), phosphorylated ZAP-70 (1:50, rabbit, Cell Signaling, Danvers, MA), vimentin (1:400, Mouse IgM, Sigma, St Louis, MO), α-tubulin (1:100, Mouse IgG1, Sigma, St Louis, MO), γ-tubulin (1:500, Rabbit, Sigma, St Louis, MO), granzyme-B (GzmB, 1:50, Rabbit, Abcam, Cambridge, UK), human CD8 (1:100, Mouse IgG2b, Serotec, Kidlington, UK), human CD4 (1:20, Mouse IgG1, Novocastra, Newcastle, UK), human CD56 (1:100, Mouse IgG1, Novocastra), human CD11b (1:100, Rat, Abcam, Cambridge, UK), and cleaved caspase-3 (cCASP3, 1:250, Rabbit, Promega, Madison, WI).

Immunohistochemical detection methods were optimized during preliminary experiments to achieve full and

homogenous antibody penetration of the whole sections. Adjacent 60-μm thick sections of each brain sample were pretreated with citrate buffer for 30 minutes at 65°C to increase antigen retrieval and penetration of the antibodies into the tissues. Sections were blocked with 1% Triton X-100 for 5 minutes and 3% normal horse serum in 0.1 M/L PBS, pH 7.4, for 60 minutes. Sections were incubated at room temperature for 48 hours with combined primary antibodies. For multiple staining, incubation with primary antibodies was followed by 4 hours of incubation with the appropriate secondary antibodies: Alexa 488, Alexa 546, Alexa 594, and/or Alexa 647 (1:1000; Molecular Probes, Carlsbad, CA). For F-actin staining sections where incubated with Alexa Fluor 488-phalloidin (1:500 in PBS; Molecular Probes) for 2 hours at room temperature after immunostaining. After washing, sections were incubated with 4,6-diamidino-2-phenylindole (DAPI) solution for 30 minutes. The sections were washed again, mounted, and examined by microscopy for normal fluorescence (Zeiss) and analyzed by confocal microscope (DMIRE2, Leica Microsystems).

Confocal Analysis

Brain sections were examined using a Leica DMIRE2 confocal microscope with a ×63 oil objective and Leica Confocal Software (Leica Microsystems). A series range for each section was set by determining an upper and lower threshold using the Z/Y Position for Spatial Image Series, and confocal microscope settings were established by Leica technicians for optimal resolution. [For further details of *in vivo* imaging of immunological synapses see previous publications].[4,20] Synapsing contacts were defined as areas where colocalization of both markers occurs between two cells in at least two 0.5-μm thick optical sections. Images can also be illustrated as they appear throughout the stack of sections as a simple 0.5-μm layer or as a transparency of all layers merged together. Randomly found synapses were captured in high resolution and analyzed in close detail to observe the pattern of distribution of CD3, α-tubulin, γ-tubulin, F-actin, and GzmB molecules in the region of intercellular contact and along the membrane. By means of the Leica confocal software, relative fluorescence intensity was quantified along the membrane in a single 0.5-μm optical section from the *z* stack at the center of the immunological synaptic interface (illustrated in the figures by arrows traversing the corresponding optical planes). Then, three-dimensional reconstructions at the interface were obtained with α blending software (Imaris, Bitplane, Zurich, Switzerland), which allowed the free rotation of the stack of images and observation of how the molecules were distributed at the interface. This three-dimensional analysis, together with the relative fluorescence analysis, permitted the type of synapses to be identified from the ring or cluster formation. The total number of synapses studied in detail with confocal microscope in this study was 157.

Confocal Quantifications and Stereology

The number of cells was estimated in the tumor areas by stereological methods using the optical fractionator probe as described previously.[21] Approximately 15 stacks of confocal images were captured and quantified per brain tumor and per cell type. Positive cells were quantified using the principle of the optical dissector.[22] Positive cells were only counted when they cut the top and left hand border of the dissector as was previously described.[22,23] The results are expressed as an estimation of the number of positive cells per mm^3, since the thickness of the sections and the number of the series of sections was considered. The density of synapsing cells was also quantified using the confocal microscope. Images containing positive cells were randomly captured from the whole tumor area. In each stack of images, the number of positive cells and the number of cells engaged in synapses were counted using stereological criteria, while the number of synapsing cells per mm^3 and their percentage of the total number of cells were calculated.

Results

Tumor Areas Are Infiltrated by T Cells That Establish Synapsing Contact with Tumor Cells

Specimens obtained from GBM patients (Figure 1) were stained for T cells and tumor cells to analyze the specific infiltration of T cells in affected areas. Tumor cells, which were detected by the expression of vimentin immunoreactivity, presented a very variable morphology (Figure 2A). Normal tissue did not show vimentin-positive ($^+$) cells and was easily differentiated from tumor tissue (Figure 2A). Since it has been shown that vimentin can also been expressed in activated macrophages,[24] a multiple immunofluorescence staining was performed combining antibodies against CD11b, vimentin and CD3. We observed that $CD11b^+$ tumor-infiltrated macrophages do not express detectable levels of vimentin (supplemental Figure S1 available at *http://ajp.amjpathol.org*).

CD3 staining revealed a massive infiltration of T cells confined to the tumor areas (Figure 2, A and B). To characterize the lymphocytes infiltrated in glioblastoma, the tumors were stained by multiple fluorescence labeling. Areas with $vimentin^+$ cells showed a specific infiltration of $CD8^+$ and $CD4^+$ T cells in all four cases studied (Figure 2, C and D), where similar proportions of $CD8^+$ and $CD4^+$ T cells were found, except in HC484 where $CD4^+$ T cells were much more numerous. $CD8^+$ T cells were observed mingled with the tumor tissue, but $CD4^+$ T cells were mainly found around blood vessels (supplemental Figure S2 available at *http://ajp.amjpathol.org*).

Multiple immunofluorescence and stereological quantification showed the evidence of TCR signaling, demonstrated by the expression of phosphorylated ZAP70

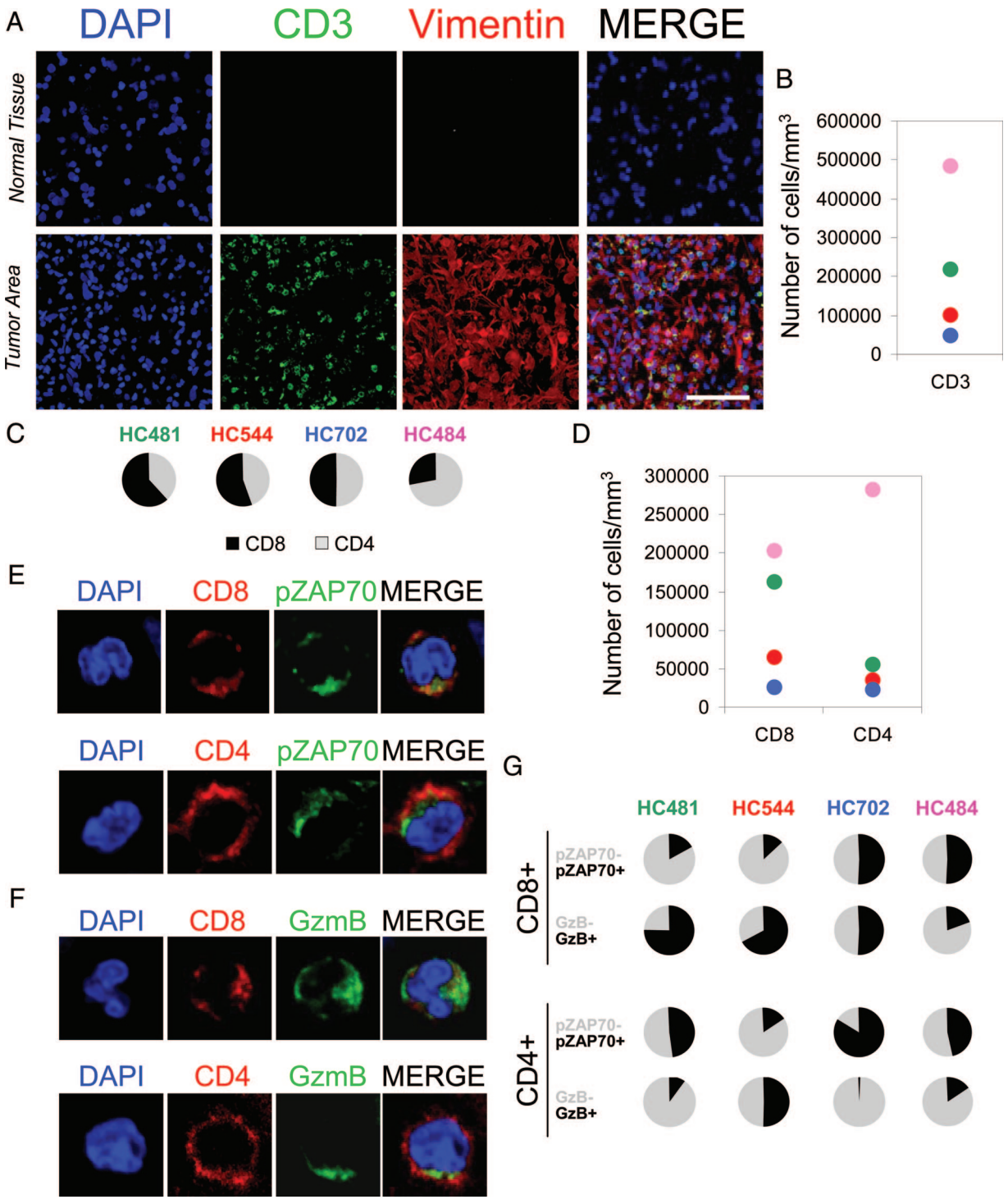

Figure 2. Tumor areas are infiltrated by T cells. **A:** Confocal pictures show normal brain tissue and a brain tumor area stained by DAPI (nuclei) as a counterstaining (blue), CD3 (green), and vimentin (red). The MERGE of the three channels is also shown. Brain tumor areas, detected by the presence of vimentin$^+$ cells, were specifically infiltrated by CD3$^+$ T cells (green). Scale bar = 100 μm. **B:** Stereological estimation of the number of infiltrated CD3$^+$ T cells by mm^3. **C:** Percentage of CD8$^+$ and CD4$^+$ T cells infiltrated in the tumor areas of all four cases studied. **D:** Stereological estimation of the density of infiltrated CD8$^+$ and CD4$^+$ cells in the tumor areas. **E**, **F**, and **G:** Representation of the characterization of tumor infiltrated T cells. The confocal pictures in **E** and **F** illustrate the staining for CD8 or CD4 (red) combined with GzmB or pZAP70 (green) and DAPI as a counterstaining (blue). The graphs in **G** show the percentages of CD8$^+$GzmB$^+$, CD8$^+$GzmB$^-$, CD8$^+$pZAP70$^+$, and CD8$^+$pZAP70$^-$, and the percentages of CD4$^+$GzmB$^+$, CD4$^+$GzmB$^-$, CD4$^+$pZAP70$^+$, and CD4$^+$pZAP70$^-$.

(pZAP70) in both CD8$^+$ and CD4$^+$ T cells (Figure 2, E and G).

Multiple staining also demonstrated that both CD8$^+$ and CD4$^+$ T cells could express GzmB in the tumor areas (Figure 2, F and G). The percentage of CD8$^+$ and CD4$^+$ cells expressing pZAP70 or GzmB per mm^3 was also estimated by stereological quantification (Figure 2G). The proportion of GzmB$^+$ and pZAP70$^+$ T cells was variable

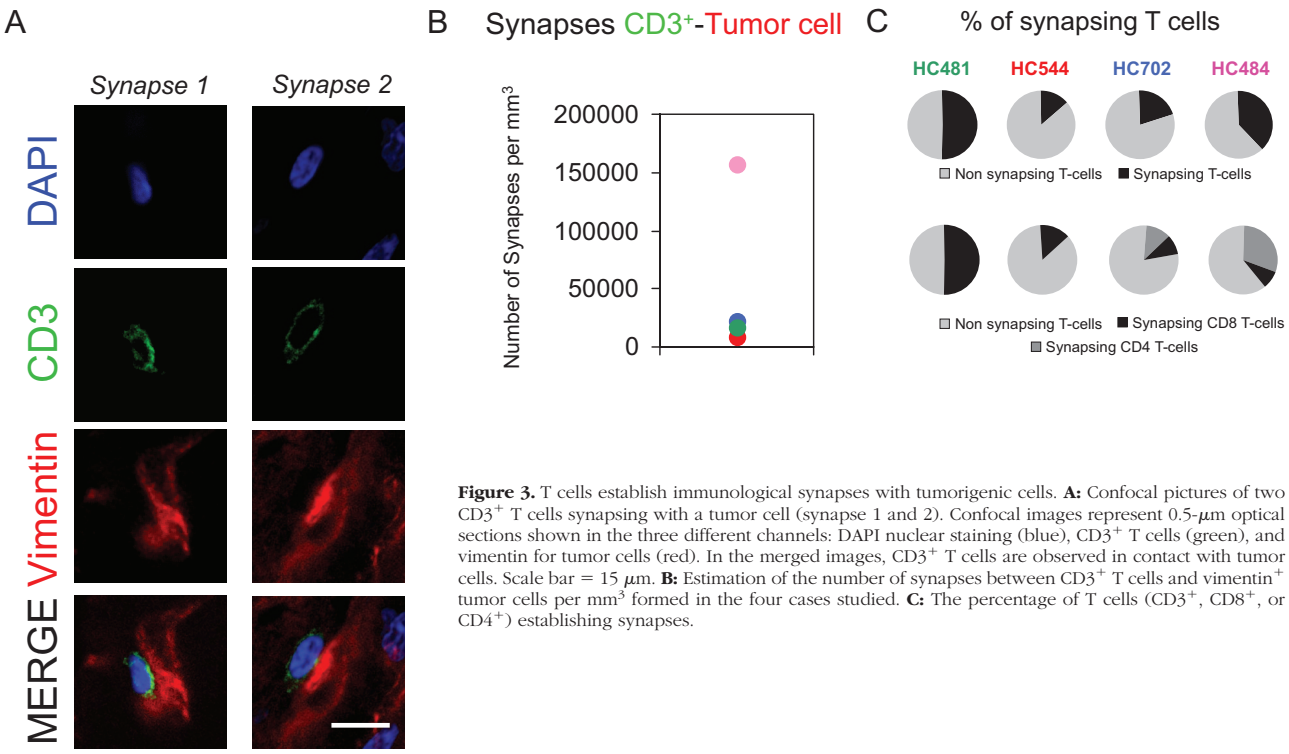

Figure 3. T cells establish immunological synapses with tumorigenic cells. **A:** Confocal pictures of two $CD3^+$ T cells synapsing with a tumor cell (synapse 1 and 2). Confocal images represent 0.5-μm optical sections shown in the three different channels: DAPI nuclear staining (blue), $CD3^+$ T cells (green), and vimentin for tumor cells (red). In the merged images, $CD3^+$ T cells are observed in contact with tumor cells. Scale bar = 15 μm. **B:** Estimation of the number of synapses between $CD3^+$ T cells and vimentin$^+$ tumor cells per mm^3 formed in the four cases studied. **C:** The percentage of T cells ($CD3^+$, $CD8^+$, or $CD4^+$) establishing synapses.

in the cases studied, ranging from a high proportion of $CD8^+$ $GzmB^+$ T cells (representing a potentially effective CTL response as in HC481) to a low proportion of $CD8^+$ $GzmB^+$ T cells (representing a poor CTL response as in HC484). Analysis of the number of tumor-infiltrated T cells per mm^3 and the age of the patients revealed that $CD3^+$ T cell infiltration increased with age, while the number of $CD8^+GzmB^+$ T cells decreased (supplemental Figure S3 available at *http://ajp.amjpathol.org*). Given that natural killer cells are also able to express pZAP70 and GzmB, a multiple immunofluorescence was performed combining antibodies against CD56, pZAP70, or GzmB, and vimentin in brain tumor sections. Since some tumors cells have been described as expressing CD56, we characterized the natural killer cells as $CD56^+$vimentin$^-$. Some natural killer cells were seen to express pZAP70 or GzmB in the tumor areas, but in lower numbers than T cells (supplemental Figure S1B available at *http://ajp.amjpathol.org*).

Areas of T cell infiltration were then analyzed in detail by confocal microscopy. $CD3^+$ T cells were found synapsing with tumor cells in all of the samples studied (Figure 3, A and B). Similarly, $pZAP70^+$ cells were also found in contact with tumor cells (supplemental Figure S4 available at *http://ajp.amjpathol.org*). All four cases showed $CD8^+$ T cells establishing synapses with tumor cells but only two of them (case HC484 and HC702) showed $CD4^+$ synapsing T cells (Figure 3C). $CD8^+$ synapsing T cells were normally found in parenchyma and blood vessels in all four cases but $CD4^+$ synapsing T cells were mainly found in the perivascular compartment (especially high in case HC484).

Polarization of GzmB Immunoreactivity toward Brain Tumor Cells in $CD8^+$ T Cells

Since GzmB is one of the key effector molecules involved in the CTL-mediated killing and clearance of tumor cells,[10,25] we analyzed in detail the $CD8^+GzmB^+$ synapsing T cells. Imaging of the $CD8^+$ T cells in contact with tumor cells showed polarization of the GzmB immunoreactivity toward the tumor cells (Figure 4A). GzmB was observed polarized and was located in the nuclear notch formed in $CD8^+$ T cells (Figure 4, B and C). Quantification of the percentage of the $CD8^+GzmB^+$ synapsing T cells revealed a low percentage of synapses in all four cases studied (Figure 4C).

MTOC of T Cells Is Polarized toward Tumor Cells in Human GBM

As is known, MTOC polarization is needed for effective CTL immunological synapse and the release of cytolytic granules.[5,7] We therefore studied the localization of MTOC in infiltrated $CD8^+$ T cells and $CD4^+$ T cells, as evidenced by the accumulation of γ-Tubulin immunoreactivity. Detailed confocal analysis demonstrated that $CD8^+$ and $CD4^+$ T cells infiltrating the tumor re-

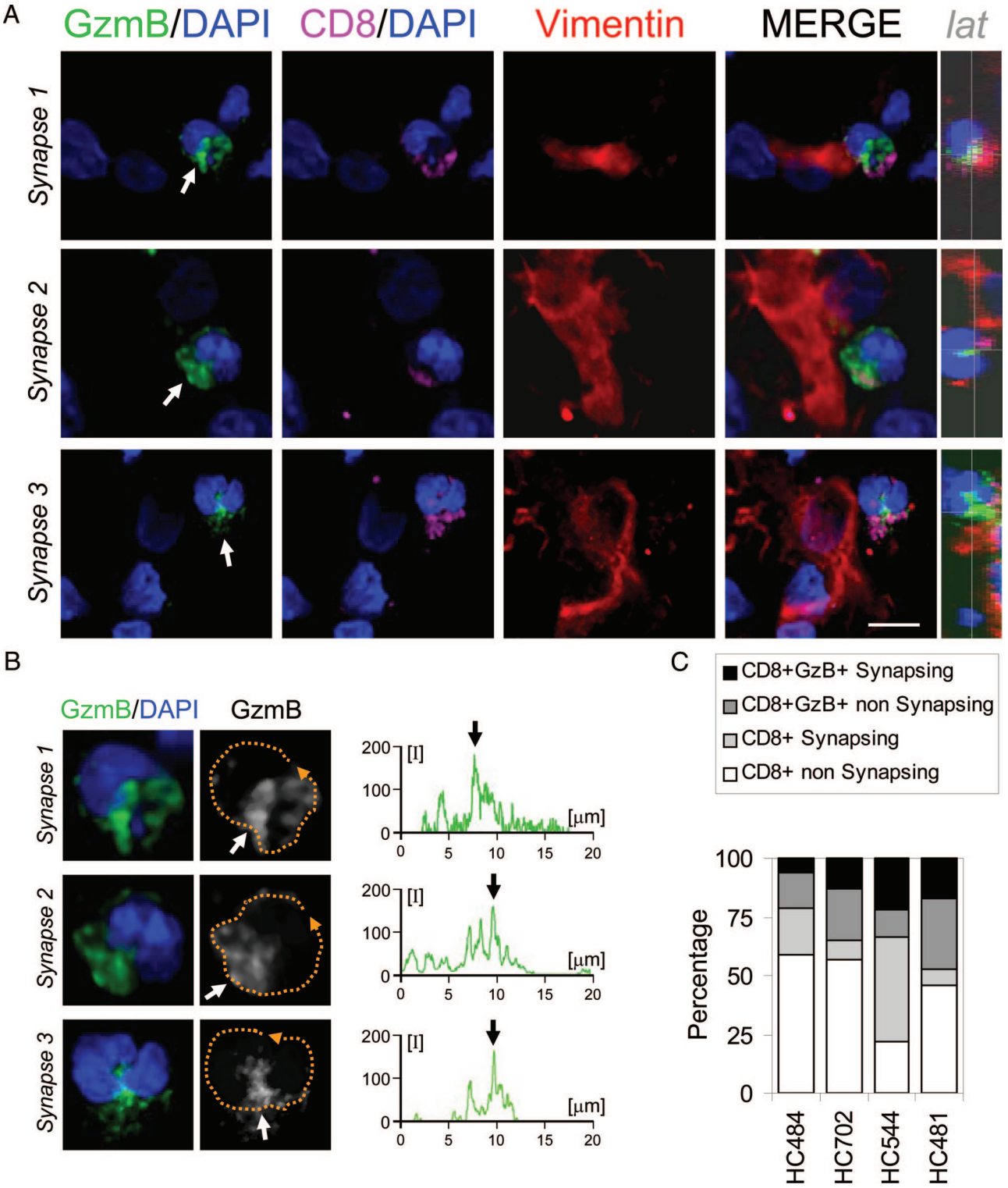

Figure 4. Polarization of GzmB toward tumor cells in CTL. Panel **A** illustrates three synapses between a $CD8^+$ T cell and a human GBM tumor cell. Confocal images of GzmB (green), CD8 (magenta), and vimentin (red) combined with DAPI as a nuclear counterstaining (blue). The overlapping of all channels is also shown (MERGE). In the three cases the nuclei (DAPI) present the characteristic indentation toward the tumor cell (**arrows** in DAPI). GzmB immunoreactivity (green) is observed polarized toward the tumor cell and is located in the region of the nuclear notch (**arrows** in GzmB/DAPI). CD8 is also found polarized toward the tumor cell (CD8/DAPI). A lateral view of the perpendicular plane of the area of contact is also depicted (*lat*). Panel **B** illustrates a higher magnification of the three T cell nuclei analyzed in panel **A** combined with GzmB. It can be seen in detail that GzmB is located at the nucleus indentation in all three synapses. Measurements of the relative fluorescence were performed along the membrane of the cells (broken orange line) and are represented in the graphs. Maximum fluorescence was oriented to the area of contact and is indicated with an **arrow** in the three cases analyzed. Panel **C** shows the quantification of the percentage of CTLs synapsing with tumor cells in all four cases studied. Scale bar = 15 μm.

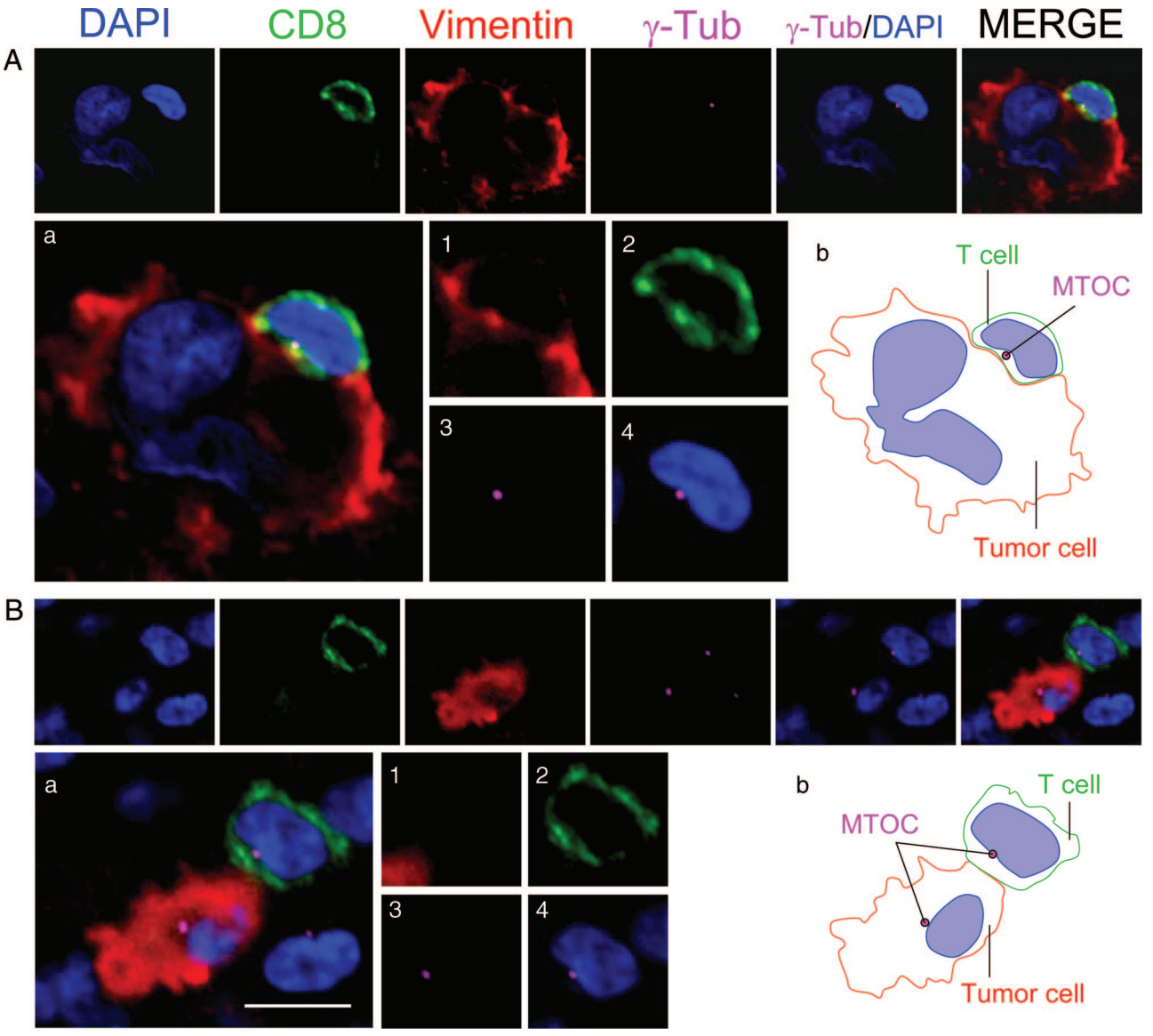

Figure 5. MTOC is polarized toward tumor cells in $CD8^+$ T cells. Two synapses between a $CD8^+$ T cell and a tumor cell are shown in detail. Each synapse was stained for nuclei (DAPI) (blue), $CD8^+$ T cells (green), vimentin (red), and MTOC (γ-Tub) (magenta). The panels illustrate three synapses between a T cell and a tumor cell. γ-Tub/DAPI and the overlapping of all four channels (MERGE) are also shown for each case. In **A**, a tumor cell with an aberrant nucleus is contacted by a $CD8^+$ T cell. A magnification of the MERGE is shown in **Aa** and the $CD8^+$ T cell is shown at higher magnification in images **1–4** [vimentin, (**1**) CD8 (**2**), γ-tubulin (**3**), and γ-tubulin+DAPI(**4**)]. The $CD8^+$ T cell(**2**) is establishing a synapsing contact with the tumor cell (**1**) and the MTOC (γ-Tub)(**3**) is oriented toward the tumor cell. The MTOC is located in the indentation that the T cell nucleus forms and is oriented toward the intercellular contact (**4**). Image **Ab** illustrates a schematic drawing of the intercellular contact. **B** illustrates another tumor cell contacted by a $CD8^+$ T cell, illustrated in the same way as in **A**. Magnification of MERGE is shown in **Ba**. Polarization of the MTOC (γ-Tub) (magenta) toward a tumor cell can be observed in T cell. The MTOC of the tumor cell can also be seen in the same optical plane. Magnification of the T cell is illustrated in images **1–4**. The $CD8^+$ T cell (**2**) in contact with the tumor cell (**1**) displays its MTOC (**3**) polarized toward the tumor cell and is also located at the notch formed by the T cell nucleus. (**4**) A schematic representation of the synapse is illustrated in **Bb**. Scale bar = 15 μm.

gion polarize their MTOC toward the tumor cells (Figure 5, A and B, and supplemental Figure S5, available at *http://ajp.amjpathol.org*). Similarly to GzmB, MTOC was usually located in the indentation or notch that the T cell nucleus forms in mature immunological synapses (Figure 5, A and B, and supplemental Figure S5 available at *http://ajp.amjpathol.org*). We occasionally observed the MTOC located in a uropod-like structure in $CD8^+$ T cells toward the intercellular contact (supplemental Figure S6 available at *http://ajp.amjpathol.org*).

T Cells in Contact with Tumor Cells Rearrange CD3 and the α-Tubulin and F-Actin Cytoskeleton

Since the MTOC drives the cytoskeleton polarization and is crucial for the formation of CD3/TCR microclusters in CTL,[8,26] we analyzed the α-tubulin distribution together with the formation of CD3/TCR clusters in T cells infiltrated in human GBM. T cells in contact with tumor cells, when analyzed in detail, were seen to

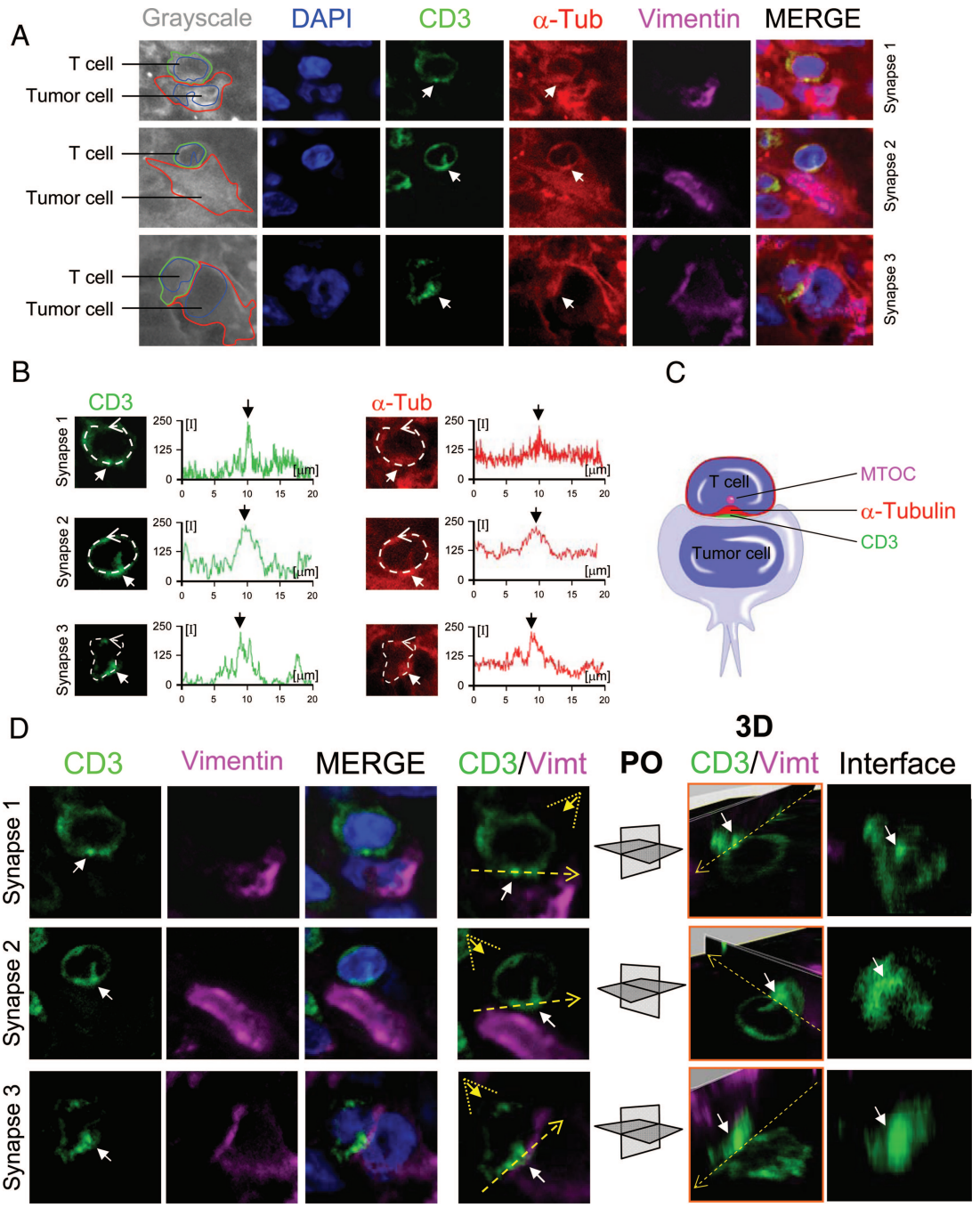

Figure 6. T cells polarize the α-tubulin cytoskeleton and form CD3 central microclusters. Confocal analysis of three synapses between T cells and tumor cells in human GBM is shown in detail. **A:** Confocal pictures of the immunohistochemistry of CD3 (green), α-tubulin (α-Tub) (red), vimentin (Vimt) (magenta), and DAPI (blue) as a counterstain. In the **left** column, the interaction between the T cell (CD3) and tumor cell (Vimt) is depicted schematically over the grayscale of α-tubulin staining (grayscale). The confocal images show three cases of synapses where CD3 and α-tubulin present an area of higher density at the center of the intercellular contact (**white arrows**). **B:** Measurements of the relative fluorescence of CD3 and α-tubulin at the membrane of the three T cells analyzed in (**A**). In all three cases, CD3 and α-tubulin have a similar pattern of fluorescence, with a higher signal at the center of the intercellular contact (**white arrows**). **C:** A schematic representation of the interaction between the T cell and the tumor cell. **D:** A three-dimensional study of the three synapses analyzed in **A** and **B**. The channels for CD3, vimentin, CD3/vimentin/DAPI (MERGE), and CD3/vimentin (CD3/Vimt) are shown. In the CD3/Vimt column of images, the plane of the interface (broken yellow line) and the angle of vision of the three-dimensional rendering (**broken yellow triangle**) is depicted. Each stack of images was rendered three dimensionally and clipped at the interface. The **white arrow** indicates the area of maximum relative fluorescence of CD3. In the column of images 3D/CD3/Vimt, the three-dimensional reconstruction of the three synapses is shown. Two perpendicular planes are illustrated crossing the interface (**broken yellow arrow**) and the area of maximum fluorescence of CD3 (**white arrow**). The plane orientation (PO) is depicted for each synapse. The plane of the intercellular contact (interface) is illustrated and the **white arrow** indicates the cluster of maximum CD3 fluorescence at the center of the interface.

rearrange their CD3 molecules and the α-tubulin cytoskeleton. The staining of CD3, α-tubulin, and vimentin combined with DAPI as a nuclear counterstaining, showed CD3 and α-tubulin to be polarized toward the tumor cell, concentrating molecules at the center of the synaptic interface (Figure 6, A and B). Furthermore CD3 formed a central supramolecular cluster at the interface between the T cell and tumor cell, as demon-

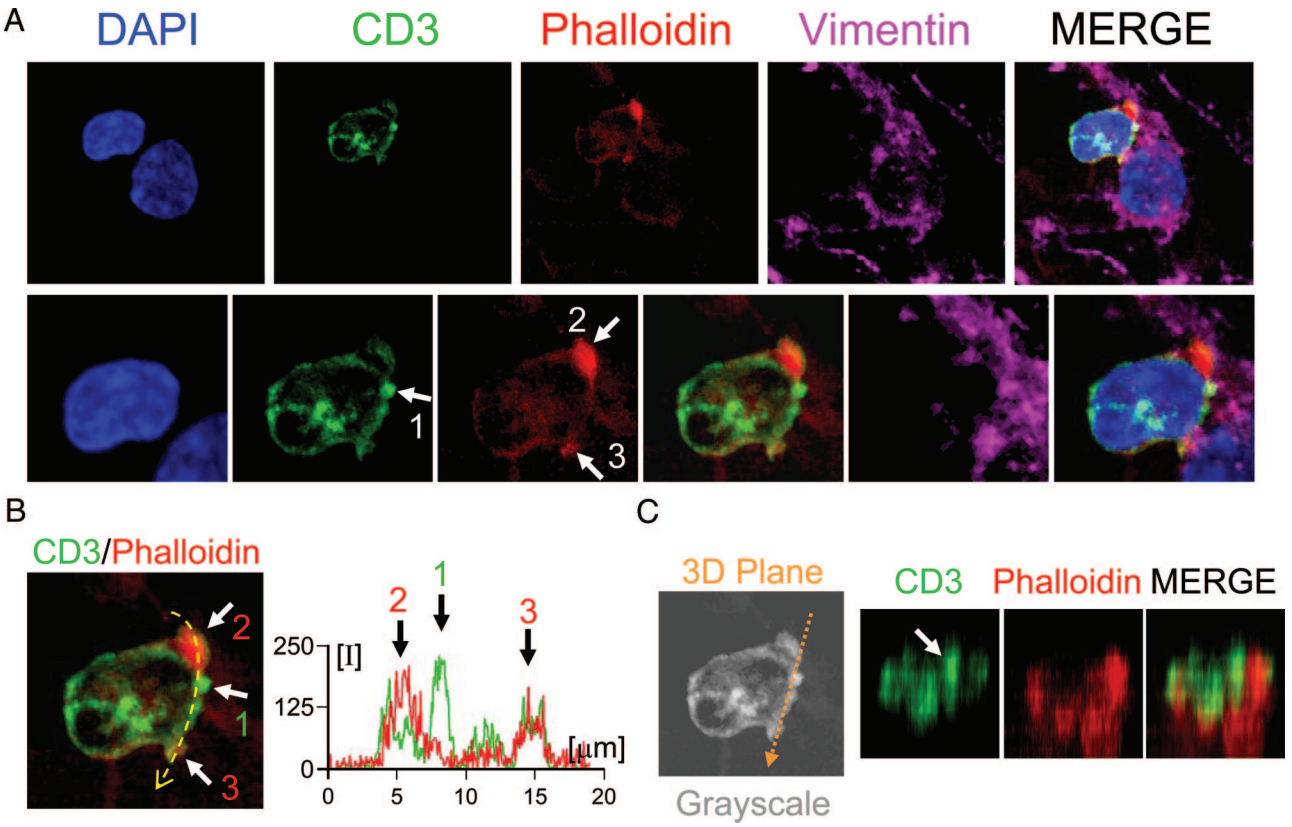

Figure 7. Central and peripheral cluster formation at T cell-Tumor cell synapse. **A:** A detailed confocal image of a T cell synapsing with a vimentin$^+$ tumor cell. In the **top row** a 1-μm optical section is shown in four different channels, DAPI for nuclei (blue), CD3 for T cells (green), phalloidin for F-actin (red), and vimentin for tumor cell (magenta). Both nuclei can be observed at the same optical plane. The **bottom row** illustrates a higher magnification of the T cell–tumor cell synapse. The CD3$^+$ T cell displays an area of high level of fluorescence at the central area of the interface (**arrow** 1). Phalloidin (F-actin) staining shows higher fluorescence at the periphery of the interface (**arrows** 2 and 3) demonstrating the *en face* orientation of the cell membrane. Panel **B** shows the merge of CD3 and phalloidin channels indicating the CD3 cluster (**arrow** 1) and F-actin cluster (**arrows** 2 and 3). The graph illustrates the quantification of the relative fluorescence of CD3 and phalloidin at the interface (indicated by the **yellow broken arrow**). The maximum peak of CD3 fluorescence is indicated by **arrow** 1 and the maximum peaks of phalloidin fluorescence are indicated by **arrows** 2 and 3. (**C**) illustrates the three dimensional reconstruction of CD3 and F-actin at the plane of the interface (the three-dimensional plane is indicated by the **broken orange arrow**). The three-dimensional reconstructions revealed a CD3 central cluster surrounded by F-actin ring.

strated by three-dimensional reconstruction (Figure 6, C and D).

Since the F-actin cytoskeleton has been described as forming a lamella around the CD3/TCR complex, in the forming of the peripheral ring,[12] we also analyzed the F-actin filaments in human GBM specimens. For this, the tumor sections were stained with phalloidin, combined with antibodies against CD3 and vimentin, and analyzed in detail the interface of the T cell–tumor cell interactions. In the area of contact, the F-actin molecules were seen to segregate three-dimensionally to the peripheral area of the intercellular interface, forming a peripheral ring surrounding the central CD3 rich area (Figure 7, A–C).

T Cells May Induce Fragmentation of the α-Tubulin Cytoskeleton in Tumor Cells

Since it is known that CTL GzmB perturbs microtubular polymerization and is able to cleave α-tubulin cytoskeleton,[27–29] we analyzed the cytoskeleton of the tumor cells in contact with T cells. It was seen that the tumor cells synapsing with T cells had an α-tubulin cytoskeleton that differed in appearance from the uniform and homogeneous α-tubulin cytoskeleton of tumor cells not in contact (Figure 8, A, B1, and B2). This alteration was characterized by the formation of α-tubulin aggregates. Confocal images of these cells showed that immunoreactivity for α-tubulin is irregular and sketchy compared with tumor cells not in contact with T cells, where the staining was regular (Figure 8A). This characteristic broken appearance of α-tubulin was classified as fragmented, and when quantifying the percentage of cells showing such an appearance (whether or not in contact with T cells), it was seen that those in contact with T cells were more likely to show a fragmented α-tubulin cytoskeleton than the tumor cells not in contact with T cells (Figure 8C).

cCASP3 Is Expressed in Tumor Areas in Cells in Contact with CD8$^+$ T Cells

Since it has been demonstrated that tumor-infiltrated CTLs are able to induce cCASP3 expression *in vivo* in animal tumor models,[16,17] we performed immunofluo-

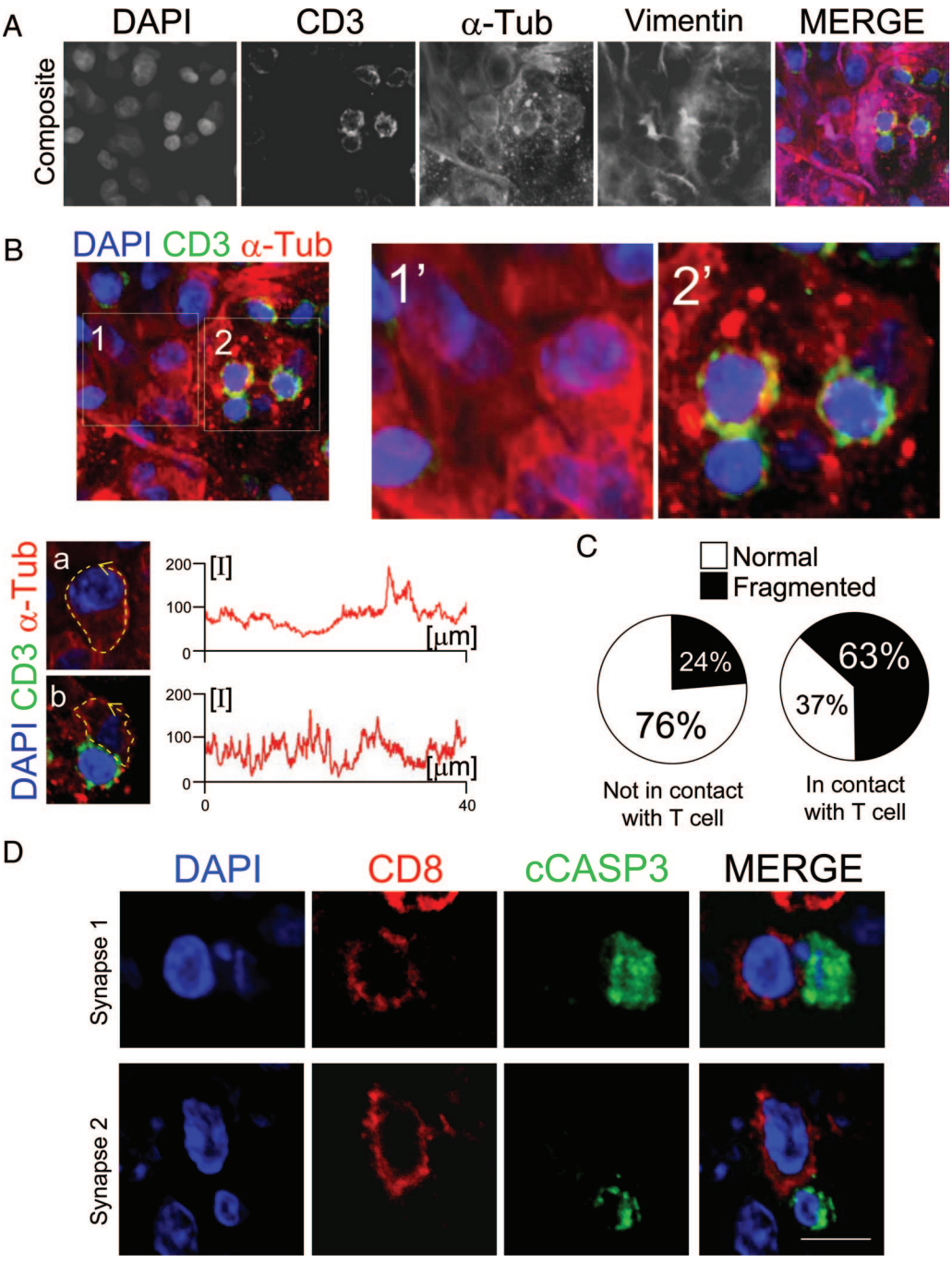

Figure 8. Cells in contact with T cells show fragmentation of the α-tubulin cytoskeleton in tumor cells and expression of cCASP3. **A:** A confocal analysis of a human GBM region stained to visualize CD3, α-tubulin, and vimentin, with DAPI as a nuclear counterstain. The overlapping of all four channels is shown in MERGE. (**B**) shows the region but only superposing the channels for DAPI, CD3, and α-tubulin. Two areas of the region are illustrated in detail (**1** and **2**). Area **1** has no T cells and area **2** has T cells. Images **1′** and **2′** show a higher magnification of areas **1** and **2**. The confocal resolution of the images is sufficient to distinguish the different appearance of the α-tubulin cytoskeleton of tumor cells whether or not they are synapsing with T cells. Graphs show the relative fluorescence measurements of α-tubulin cytoskeleton along the cell membrane (**broken yellow arrow**) of a tumor cell not in contact with T cells (**a** [cropped from **1**]) and a tumor cell in contact with a T cell (**b** [cropped from **2**]). The measurements of the relative fluorescence of α-tubulin in the cell not in contact with T cells (**a**) shows uniform fluorescence levels, while the tumor cell in contact with a T cell (**b**) displays broken fluorescence levels. **C:** The quantification of the percentage of tumor cells that present a cleaved appearance of α-tubulin, whether they are in contact or not with T cells. Pie charts show that tumor cells in contact with T cells present a cleaved α-tubulin cytoskeleton more frequently than the tumor cells not in contact with T cells (63% vs 24%). A total of 167 cells were analyzed for this quantification. **D** illustrates two $CD8^+$ T cells in contact with a $cCASP3^+$ cell. The **top row** shows a $CD8^+$ T cell in contact with a $cCASP3^+$ cell displaying a fragmented nucleus. The **bottom row** illustrates a T cell in contact with a $cCASP3^+$ cell showing a condensed and reduced nucleus. Scale bar = 15 mm.

rescence by combining antibodies against CD8 and cCASP3. We observed $cCASP3^+$ cells in the tumor areas, normally accompanied by a pyknotic or fragmented nucleus. Importantly, we observed $cCASP3^+$ cells in close apposition with $CD8^+$ cells in the glioblastoma areas (Figure 8D). Quantification revealed that 18% of the cCASP3+ cells were in contact with $CD8^+$ T cells.

Discussion

In the present work, we demonstrate that immunological synapses between CTLs and tumorigenic cells occur in human GBM, which may have important implications for brain tumor clearance. This intercellular contact is characterized by the three-dimensional segregation of the CD3/TCR complex in T cells, which forms a central cluster at the interface, and also involves the relocation and polarization of the T cell cytoskeleton, involving α and γ tubulin and F-actin. We show that $CD3^+$ T cells, infiltrated in human glioma-affected regions, are active since they show evidence of TCR signaling such as the expression of phosphorylated ZAP70. As previously described, this activation controls the clustering of CD3/TCR,[11,30] which is characterized by the formation of the central aggregate at the interface of the IS, the so-called central supramolecular activation cluster.[6] Our immunofluorescence studies demonstrated that the three-dimensional accumulation of CD3/TCR at the interface of antitumor CTLs coincides with the re-arrangements of α-tubulin microtubules. Analysis of the relative fluorescence reveals that polarization of the microtubules and CD3/TCR follows a very similar pattern (Figure 6), suggesting that central supramolecular activation cluster is facilitated by α-tubulin relocation.

Our confocal images also show that MTOC relocates toward the interface and may drive and polarize the α-tubulin microtubules toward the tumorigenic cell (Figure 5). Previous studies performed in cell cultures, using high resolution images and three-dimensional reconstruction, demonstrated that microtubules undergo polarization driven by the MTOC in T cells.[8] Our studies showed a similar distribution pattern of α-tubulin in the T cells in contact with tumor cells, although the resolution of our images *in situ* in human specimens was not sufficient for the fine tubular structure to be appreciated. Furthermore, the microtubules of surrounding cells hinder the more precise three-dimensional reconstruction of the samples.

Our images also show that F-actin filaments form a ring surrounding the central CD3/TCR cluster (Figure 7). This finding correlates with previous studies described *in vitro* in Jurkat T cells where a F-actin ring matches with the peripheral supramolecular activation cluster formed by LFA-1 and its distribution contributes to the shape and maintenance of the characteristic bull's-eye pattern of the immunological synapse.[12] F-actin filaments are linked to LFA-1 molecules through Talin molecules and the interaction between these molecules appears to be crucial for the rearrangements of adhesion molecules at the synaptic interface.[12,31,32]

Of all of the TIL populations studied in the present work, CTL ($CD8^+GzmB^+$) may be relevant for brain tumor clearance and is probably the only T cell subset able to mediate an effective immune response and remit the tumor mass. However, the percentage of CTL synapses was very low in all cases, suggesting a deficient immunological response in GBM (Figure 4). On the other hand, $CD4^+$ T cells were mostly found in the perivascular area and not all GBM cases showed $CD4^+$ synapsing T cells (Figure 3 and supplemental Figure S2 available at *http://ajp.amjpathol.org*). Previous studies, both from our group and others, have found similar results regarding the anatomical position of $CD4^+$ T cells, which seems to be crucial for the effectiveness of the immune response.[4,33] The function of the $CD4^+$ T cells in blood vessels is unclear, but they may help entry of the effector CTL into the tissue.

$CD8^+$ T cells synapsing with tumor cells are seen to express GzmB as effector molecule, which is polarized toward the interface (Figure 4). This result suggests that the polarization of GzmB in $CD8^+$ T cells may be crucial for an immune-mediated antitumor response in human GBM. Importantly, our images also show that the nucleus of T cells establishing IS very often presents a particular shape, consisting of an indentation oriented to the target cell (Figure 4C). Both MTOC and GzmB immunoreactivity are located in this notch (Figures 4 and 5 and supplemental Figure S5 available at *http://ajp.amjpathol.org*). This nuclear appearance suggests that α-tubulin microtubules, anchored in MTOC and the membrane, may drag the cell toward the interface, changing the nuclear morphology, concentrating the cytoplasm and forming a chamber-like compartment toward the target cell. Since MTOC polarization at IS is essential for the delivery of secretory granules,[7] this nuclear appearance may be caused by the dynamics of microtubules and could explain how MTOC polarization provides a mechanism for concentrating secretory vesicles on a particular target.[34]

Interestingly, our confocal images show that both $CD8^+$ and $CD4^+$ T cells relocate the MTOC toward target cells (Figure 5 and supplemental Figure S5 available at *http://ajp.amjpathol.org*). Both $CD8^+$ and $CD4^+$ T cells may display similar arrangements of clusters and cytoskeleton.[35] However, $CD8^+$ T cells are more likely to be found since they are more inclined to form rings than $CD4^+$ T cells.[36] Given also the fact that $CD4^+$ T cells are mainly located in the blood vessels and only two of the cases showed synapsing $CD4^+$ T cells, we believe that the formation of these molecular arrangements in GBM may be more frequent in $CD8^+$ T cells. In addition, since $CD4^+$ T cells intervene in regulatory processes of the immune response, the study of T cell–T cell interactions in GBM may well deserve further analysis in the future.

We also demonstrated here that a large proportion of tumor cells in contact with T cells show alteration of the α-tubulin microtubules. This finding is in line with previous reports demonstrating that, *in vitro*, GzmB targets the cytoskeleton and alters microtubule polymerization.[27,37] In fact, α-tubulin has been described as a physiological substrate for GzmB in CTL-mediated apoptosis.[28] It is not fully understood why GzmB cleaves α-tubulin and what consequences there may be for the target cell.[29] It has been proposed that GzmB delivered to target cells may induce cell death mediated by α-tubulin cleavage,[27,28] but another effect of the GzmB mediated cleavage of α-tubulin may be to prevent cellular reorganization or to prevent the proliferation of tumor cells.[29] In view of our results, it seems that GzmB-mediated CTLs may try to arrest tumor growth in human GBM through α-tubulin

fragmentation, although the response is evidently not sufficient to cause the tumor mass to remit.

Finally, our images show the expression of cCASP3 in the tumor areas, where cCASP3-expressing cells display a very small nucleus, fragmented and/or with condensed chromatin (Figure 8D). In some cases cCASP3$^+$ cells were found isolated, close to CD8$^+$ T cells but, importantly, in contact with CD8$^+$ T cells (Figure 8D).

The three-dimensional segregation of CD3/TCR and the rearrangement of cytoskeleton observed in T cells, together with the evidence of ZAP70 phosphorylation in human GBM, suggest that T cells are able to detect and recognize a specific antigen capable of activating TCR signaling. A non-antigen-specific response is also involved in the clearance of GBM. In fact, we observed infiltration of natural killer cells, the major components of the innate immune system, but their level of homing is very low compared with the CD3$^+$ T cell infiltration (see supplemental Figure S2 available at *http://ajp.amjpathol.org*). The fact that CD3/TCR central clusters are formed in GBM suggests that the CTL response observed may be antigen-specific. Although it is known that the formation of other clusters, such as the LFA-1/Talin ring junction, can be observed in non-antigen-specific responses, the polarization and granule translocation to the interface seem to be only triggered by antigen recognition.[36] The formation of rings may have implications for the mechanism of effective CTL hunting for antigen in tissues, but we consider that CD3/TCR polarization suggests antigen-specific response.

Antitumor immune response has been described in many human cancers and it has been demonstrated that some tumor antigens induce a specific T cell response.[38] However, the action of this antigen-specific immune response seems to be blocked or altered by not very well understood mechanisms. One of the possibilities that could explain tumor tolerance is the alteration of IS formation. CTLs obtained from infiltrated tumors in mice show alterations of the mechanisms driving the polarization of the cell, such as a defective MTOC, which results in deficient IS formation.[39] In contrast with this experimental observation, we observed the normal accumulation of γ-tubulin in T cells and also the polarization of MTOC in CD8$^+$ T cells toward tumor cells. Defective MTOC does not necessarily mean the impossibility of synapse formation but, more likely, a defect in or a lower rate of IS formation.

It has also been postulated that unbalanced regulation of the T cell population could contribute to tumor growth. Patients with GBM show deficiencies in CTL and an increased population of regulatory T cells.[40–42] In the present work, we observe an infiltration of CD4$^+$GzmB$^+$ T cells that could correspond to regulatory T cells. In this way, CTLs would attempt to destroy the tumor cells, while regulatory T cells would struggle to stop the action of the CTLs. Indeed, experimental studies have demonstrated that blocking regulatory T cells facilitates the anti-tumor CTL action, resulting in tumor clearance.[25,43]

In summary, a strategy for tumor immunotherapy would involve stimulating the action of the CTLs on tumorigenic cells. This stimulation should facilitate TCR signaling, the formation of three dimensional microclusters and the segregation of GzmB granules toward intercellular contact with tumorigenic cells. Importantly, recent experimental studies performed in mice have demonstrated that the stimulation of IS formation results in a potent tumor rejection involving GzmB polarization.[44] The demonstration here that CD8$^+$ T cells establish GzmB-mediated IS with tumorigenic cells in human GBM points the way toward strategies for tumor immunotherapy and identifies potential molecular targets,[45–47] which will permit the stimulation of CTL synapse formation.

Acknowledgments

We thank all of the personnel from SAI (*Servicio de Apoyo a la Investigación*), for the help provided at the University of Murcia, especially to María García. We also thank Mr. Philip Thomas for comments and language suggestions on this manuscript. This work is dedicated to the memory of Santiago Barcia-Cozar (8 August 2006-11 November 2006).

References

1. Bossi G, Griffiths GM: CTL secretory lysosomes: biogenesis and secretion of a harmful organelle. Semin Immunol 2005, 17:87–94
2. Stinchcombe JC, Bossi G, Booth S, Griffiths GM: The immunological synapse of CTL contains a secretory domain and membrane bridges. Immunity 2001, 15:751–761
3. Stinchcombe JC, Griffiths GM: The role of the secretory immunological synapse in killing by CD8+ CTL. Semin Immunol 2003, 15:301–305
4. Barcia C, Thomas CE, Curtin JF, King GD, Wawrowsky K, Candolfi M, Xiong WD, Liu C, Kroeger K, Boyer O, Kupiec-Weglinski J, Klatzmann D, Castro MG, Lowenstein PR: In vivo mature immunological synapses forming SMACs mediate clearance of virally infected astrocytes from the brain. J Exp Med 2006, 203:2095–2107
5. Combs J, Kim SJ, Tan S, Ligon LA, Holzbaur EL, Kuhn J, Poenie M: Recruitment of dynein to the Jurkat immunological synapse. Proc Natl Acad Sci USA: 2006, 103:14883–14888
6. Monks CR, Freiberg BA, Kupfer H, Sciaky N, Kupfer A: Three-dimensional segregation of supramolecular activation clusters in T cells. Nature 1998, 395:82–86
7. Stinchcombe JC, Majorovits E, Bossi G, Fuller S, Griffiths GM: Centrosome polarization delivers secretory granules to the immunological synapse. Nature 2006, 443:462–465
8. Kuhn JR, Poenie M: Dynamic polarization of the microtubule cytoskeleton during CTL-mediated killing. Immunity 2002, 16:111–121
9. Dustin ML: A dynamic view of the immunological synapse. Semin Immunol 2005, 17:400–410
10. Lieberman J: The ABCs of granule-mediated cytotoxicity: new weapons in the arsenal. Nat Rev Immunol 2003, 3:361–370
11. Yokosuka T, Sakata-Sogawa K, Kobayashi W, Hiroshima M, Hashimoto-Tane A, Tokunaga M, Dustin ML, Saito T: Newly generated T cell receptor microclusters initiate and sustain T cell activation by recruitment of Zap70 and SLP-76. Nat Immunol 2005, 6:1253–1262
12. Kaizuka Y, Douglass AD, Varma R, Dustin ML, Vale RD: Mechanisms for segregating T cell receptor and adhesion molecules during immunological synapse formation in Jurkat T cells. Proc Natl Acad Sci USA 2007, 104:20296–20301
13. Carpentier AF, Meng Y: Recent advances in immunotherapy for human glioma. Curr Opin Oncol 2006, 18:631–636
14. Egen JG, Kuhns MS, Allison JP: CTLA-4: new insights into its biological function and use in tumor immunotherapy. Nat Immunol 2002, 3:611–618
15. Boissonnas A, Fetler L, Zeelenberg IS, Hugues S, Amigorena S: In

vivo imaging of cytotoxic T cell infiltration and elimination of a solid tumor. J Exp Med 2007, 204:345–356
16. Breart B, Lemaitre F, Celli S, Bousso P: Two-photon imaging of intratumoral CD8+ T cell cytotoxic activity during adoptive T cell therapy in mice. J Clin Invest 2008, 118:1390–1397
17. Mrass P, Takano H, Ng LG, Daxini S, Lasaro MO, Iparraguirre A, Cavanagh LL, von Andrian UH, Ertl HC, Haydon PG, Weninger W: Random migration precedes stable target cell interactions of tumor-infiltrating T cells. J Exp Med 2006, 203:2749–2761
18. Barcia C, Jimenez-Dalmaroni M, Kroeger KM, Puntel M, Rapaport AJ, Larocque D, King GD, Johnson SA, Liu C, Xiong W, Candolfi M, Mondkar S, Ng P, Palmer D, Castro MG, Lowenstein PR: One-year expression from high-capacity adenoviral vectors in the brains of animals with pre-existing anti-adenoviral immunity: clinical implications. Mol Ther 2007, 15:2154–2163
19. Thomas CE, Abordo-Adesida E, Maleniak TC, Stone D, Gerdes, G, Lowenstein PR: Gene transfer into rat brain using adenoviral vectors. Edited by JN Gerfen, R McKay, MA Rogawski, DR Sibley, and P Skolnick. New York NY, John Wiley and Sons, New York, 2000, pp. 4.23.21–24.23.40
20. Barcia C, Wawrowsky K, Barrett RJ, Liu C, Castro MG, Lowenstein PR: In vivo polarization of IFN-{gamma} at Kupfer and non-Kupfer immunological synapses during the clearance of virally infected brain cells. J Immunol 2008, 180:1344–1352
21. Barcia C, Sanchez Bahillo A, Fernandez-Villalba E, Bautista V, Poza YPM, Fernandez-Barreiro A, Hirsch EC, Herrero MT: Evidence of active microglia in substantia nigra pars compacta of parkinsonian monkeys 1 year after MPTP exposure. Glia 2004, 46:402–409
22. Sterio DC: The unbiased estimation of number and sizes of arbitrary particles using the dissector. J Microsc 1984, 134 (Pt 2):127–136
23. Barcia C, Gomez A, de Pablos V, Fernandez-Villalba E, Liu C, Kroeger KM, Martin J, Barreiro AF, Castro MG, Lowenstein PR, Herrero MT: CD20, CD3, and CD40 ligand microclusters segregate three-dimensionally in vivo at B-cell-T-cell immunological synapses after viral immunity in primate brain. J Virol 2008, 82:9978–9993
24. Mor-Vaknin N, Punturieri A, Sitwala K, Markovitz DM: Vimentin is secreted by activated macrophages. Nat Cell Biol 2003, 5:59–63
25. Cao X, Cai SF, Fehniger TA, Song J, Collins LI, Piwnica-Worms DR, Ley TJ: Granzyme B and perforin are important for regulatory T cell-mediated suppression of tumor clearance. Immunity 2007, 27:635–646
26. Martin-Cofreces NB, Sancho D, Fernandez E, Vicente-Manzanares M, Gordon-Alonso M, Montoya MC, Michel F, Acuto O, Alarcon B, Sanchez-Madrid F: Role of Fyn in the rearrangement of tubulin cytoskeleton induced through TCR. J Immunol 2006, 176:4201–4207
27. Adrain C, Duriez PJ, Brumatti G, Delivani P, Martin SJ: The cytotoxic lymphocyte protease, granzyme B, targets the cytoskeleton and perturbs microtubule polymerization dynamics. J Biol Chem 2006, 281:8118–8125
28. Goping IS, Sawchuk T, Underhill DA, Bleackley RC: Identification of {alpha}-tubulin as a granzyme B substrate during CTL-mediated apoptosis. J Cell Sci 2006, 119:858–865
29. Waterhouse NJ, Oliaro J, Pinkoski MJ: A 'polarized' look at alpha-tubulin cleavage by granzyme B. Cell Death Differ 2006, 13:1839–1841
30. Blanchard N, Di Bartolo V, Hivroz C: In the immune synapse. ZAP-70 controls T cell polarization and recruitment of signaling proteins but not formation of the synaptic pattern. Immunity 2002, 17:389–399
31. Nolz JC, Gomez TS, Zhu P, Li S, Medeiros RB, Shimizu Y, Burkhardt JK, Freedman BD, Billadeau DD: The WAVE2 complex regulates actin cytoskeletal reorganization and CRAC-mediated calcium entry during T cell activation. Curr Biol 2006, 16:24–34
32. Huang Y, Burkhardt JK: T-cell-receptor-dependent actin regulatory mechanisms. J Cell Sci 2007, 120:723–730
33. Stohlman SA, Bergmann CC, Lin MT, Cua DJ, Hinton DR: CTL effector function within the central nervous system requires CD4+ T cells. J Immunol 1998, 160:2896–2904
34. Kupfer A, Dennert G, Singer SJ: The reorientation of the Golgi apparatus and the microtubule-organizing center in the cytotoxic effector cell is a prerequisite in the lysis of bound target cells. J Mol Cell Immunol 1985, 2:37–49
35. Lin J, Miller MJ, Shaw AS: The c-SMAC: sorting it all out (or in). J Cell Biol 2005, 170:177–182
36. Somersalo K, Anikeeva N, Sims TN, Thomas VK, Strong RK, Spies T, Lebedeva T, Sykulev Y, Dustin ML: Cytotoxic T lymphocytes form an antigen-independent ring junction. J Clin Invest 2004, 113:49–57
37. Bredemeyer AJ, Lewis RM, Malone JP, Davis AE, Gross J, Townsend RR, Ley TJ: A proteomic approach for the discovery of protease substrates. Proc Natl Acad Sci USA 2004, 101:11785–11790
38. Sahin U, Tureci O, Pfreundschuh M: Serological identification of human tumor antigens. Curr Opin Immunol 1997, 9:709–716
39. Radoja S, Saio M, Schaer D, Koneru M, Vukmanovic S, Frey AB: CD8(+) tumor-infiltrating T cells are deficient in perforin-mediated cytolytic activity due to defective microtubule-organizing center mobilization and lytic granule exocytosis. J Immunol 2001, 167:5042–5051
40. Fecci PE, Mitchell DA, Whitesides JF, Xie W, Friedman AH, Archer GE, Herndon JE, 2nd, Bigner DD, Dranoff G, Sampson JH: Increased regulatory T-cell fraction amidst a diminished CD4 compartment explains cellular immune defects in patients with malignant glioma. Cancer Res 2006, 66:3294–3302
41. Learn CA, Fecci PE, Schmittling RJ, Xie W, Karikari I, Mitchell DA, Archer GE, Wei Z, Dressman H, Sampson JH: Profiling of CD4+, CD8+, and CD4+CD25+CD45RO+FoxP3+ T cells in patients with malignant glioma reveals differential expression of the immunologic transcriptome compared with T cells from healthy volunteers. Clin Cancer Res 2006, 12:7306–7315
42. Parsa AT, Waldron JS, Panner A, Crane CA, Parney IF, Barry JJ, Cachola KE, Murray JC, Tihan T, Jensen MC, Mischel PS, Stokoe D, Pieper RO: Loss of tumor suppressor PTEN function increases B7-H1 expression and immunoresistance in glioma. Nat Med 2007, 13:84–88
43. Piconese S, Valzasina B, Colombo MP: OX40 triggering blocks suppression by regulatory T cells and facilitates tumor rejection. J Exp Med 2008, 205:825–839
44. Stephan MT, Ponomarev V, Brentjens RJ, Chang AH, Dobrenkov KV, Heller G, Sadelain M: T cell-encoded CD80 and 4-1BBL induce auto- and transcostimulation, resulting in potent tumor rejection. Nat Med 2007, 13:1440–1449
45. Curtin JF, King GD, Candolfi M, Greeno RB, Kroeger KM, Lowenstein PR, Castro MG: Combining cytotoxic and immune-mediated gene therapy to treat brain tumors. Curr Top Med Chem 2005, 5:1151–1170
46. King GD, Curtin JF, Candolfi M, Kroeger K, Lowenstein PR, Castro MG: Gene therapy and targeted toxins for glioma. Curr Gene Ther 2005, 5:535–557
47. King GD, Muhammad AK, Curtin JF, Barcia C, Puntel M, Liu C, Honig SB, Candolfi M, Mondkar S, Lowenstein PR, Castro MG: Flt3L and TK gene therapy eradicate multifocal glioma in a syngeneic glioblastoma model. Neuro Oncol 2008, 10:19–31